Tunnel Currents across Silane Diamines/Dithiols and Alkane Diamines/Dithiols: A Comparative Computational Study

ARTICLE *in* THE JOURNAL OF PHYSICAL CHEMISTRY C · JANUARY 2009

Impact Factor: 4.77 · DOI: 10.1021/jp8078698

5 AUTHORS, INCLUDING:

Giorgos Fagas
Tyndall National Institute
76 PUBLICATIONS **1,049** CITATIONS
SEE PROFILE

Mark A. Ratner
Northwestern University
906 PUBLICATIONS **42,537** CITATIONS
SEE PROFILE

Tunnel Currents across Silane Diamines/Dithiols and Alkane Diamines/Dithiols: A Comparative Computational Study

Shane McDermott,[†] Christopher B. George,*[,‡] Giorgos Fagas,[†] James C. Greer,[†] and Mark A. Ratner[‡]

Tyndall National Institute, Lee Maltings, Prospect Row, Cork, Ireland, and Department of Chemistry, Northwestern University, Evanston, Illinois 60208, USA

Received: September 4, 2008; Revised Manuscript Received: November 4, 2008

Two different first-principles methods, one based on density functional theory combined with Green's functions and the other on a configuration interaction method, are used to calculate the electronic transport properties of alkane and silane chains terminated by amine end groups in metal−molecule−metal junctions. The low-voltage conductance is found to decay exponentially with increasing length in both systems, and decay constants are obtained from the different methods. Both methods predict smaller conductance values and steeper decay in the alkane-bridged junctions compared with the silane-bridged junctions, but quantitative differences in the decay constants obtained from the two formalisms arise. These differences are attributed to the treatment of the energy-level alignments in the tunnel junctions as well as the treatment of correlation within the molecular chains. Additionally, end-group effects for both the alkane and the silane chains are studied using both a simple tunnel barrier model and complex band-structure calculations. These results are used to explain differences observed in conductance decay constants in amine- and thiol-linked junctions obtained from the two transport methods; the results further highlight the importance of accurate energy-level alignment between the electrode and molecular states.

I. Introduction

As a central problem of molecular electronics, the process of electron transport through single molecules between metallic electrodes has been achieved experimentally and studied theoretically.[1–3] The desire to create junctions with tailored functionalities has led to work examining the roles that end groups, molecular energy levels, and contact geometries play in determining the transport properties of these systems.[4–14] In particular, recent studies have examined physical tunnel junctions in which alkanes of varying lengths are bonded between gold electrodes via amine or thiol linkers.[5,10,15–21] These junctions exhibit an exponential decrease in low-voltage conductance, g, with increasing bridging molecular length, l (given in angstroms or the number of methylene units), as is reasonable for conductance far from any injection resonance. This behavior is described by:

$$g(l) = g_C \exp(-\beta l) \quad (1)$$

which is characterized by two parameters: the contact resistance $R_C = 1/g_c$ and the inverse decay length β[22]. The inverse decay length determines how tunnel conductance and resistance scale with increasing molecular length. The contact resistance is obtained in the limit $l \rightarrow 0$ and determines the resistance associated with the bonding of the end groups to the metal electrodes or contacts. However, the contact resistance is strongly dependent on the exact configuration of the metal−molecule bonding site,[4,8,9] so it will not be discussed in depth in this article (cf. Supporting Information).

Most theoretical treatments of conductance in single-molecule junctions up to this point have been based on density functional theory (DFT) combined with a nonequilibrium Green's function (NEGF) formalism.[23] The NEGF/DFT formalism recently has been questioned, however, over concerns that exchange-correlation effects are leading to spurious conductance values,[24–30] sometimes described incorrectly by orders of magnitude.[24] To avoid issues related to exchange-correlation approximations in DFT, a new transport formalism was recently developed.[31,32] The method uses a configuration interaction (CI) method[33,34] to calculate the electronic structure of the junction, and transport properties are calculated using the Wigner function within open boundary conditions under constraint of the maximum entropy principle.

To compare the two methodologies, four test systems were chosen. The amine- and thiol-linked systems were selected as a means to compare the effect of different end groups on conductance, whereas the silane and alkane chains were selected to compare the effects of different chemical backbones and degrees of correlation on the transport. The increased correlation in the silane chains is related to the σ-bond delocalization that has been studied extensively in peralkylated oligosilane chains.[35,36] The photophysics of these oligosilane chains has indicated that their excitation energies are lower than those of alkane chains, and the size of the band gap in silanes may lead to interesting conductance properties such as a decay length between that of alkanes and π-conjugated systems.

II. Computational Methods and Theory

Junction Geometries. Calculations are performed on tunnel junctions consisting of single molecules spanning a gap between two metal clusters. The molecules considered within this study are alkanes and silanes, and both deprotonated thiol (−S−) and

* To whom correspondence should be addressed. E-mail: shane.mcdermott@tyndall.ie (S.M.), c-george@northwestern.edu (C.B.G.), georgios.fagas@tyndall.ie (G.F.), jim.greer@tyndall.ie (J.C.G.), ratner@chem.northwestern.edu (M.A.R.).
[†] Tyndall National Institute.
[‡] Northwestern University.

10.1021/jp8078698 CCC: $40.75
Published on Web 12/16/2008

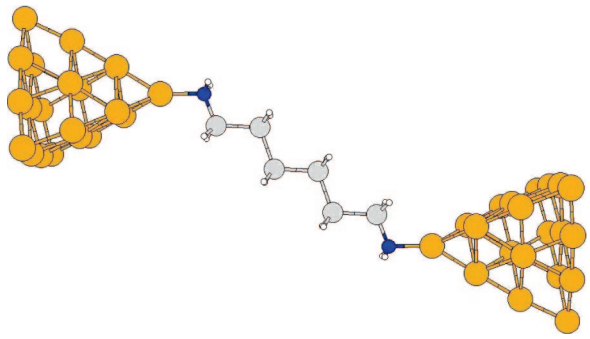

Figure 1. Representative tunnel junction model: depicted is the $Au_{20}-NH_2-(SiH_2)_6-NH_2-Au_{20}$ junction. An additional 5 × 5 layer of gold atoms (not shown) is placed on either side of the above junction for the NEGF/DFT calculations to allow for periodic DFT calculations.

amine ($-NH_2-$) end groups are used to bond the molecular chains $(-CH_2-)_n$ and $(-SiH_2-)_n$ to the gold electrodes. A typical geometry is shown in Figure 1. For thiol end groups, the electrodes are modeled as a 19 gold atom cluster, allowing the thiol to bond to a 3-atom (hollow) site.[37,38] For amine−gold bonding, a 20-atom cluster is used, allowing the $-NH_2-$ linker group to bond to a single gold apex atom.[20,39] Details of the generation of the $Au_{19}-S-(CH_2)_n-S-Au_{19}$ and $Au_{19}-S-(SiH_2)_n-S-Au_{19}$ model structures can be found in ref 37, and $Au_{20}-NH_2-(CH_2)_n-NH_2-Au_{20}$ model structures are described in ref 39.

For the comparisons presented in this work, additional tunnel junctions $Au_{20}-NH_2-(SiH_2)_n-NH_2-Au_{20}$, with $n = 4$, 6, 8, and 10, are generated; a typical junction model is shown for $n = 6$ in Figure 1. For silanes with amine end groups, molecular geometries are relaxed in the model junction with DFT calculations using the B3-LYP hybrid exchange/correlation functional[40,41] as implemented in the *TURBOMOLE* program system.[42] A split-valence polarized SV(P) basis set[43] is used for all atoms. This treats all electrons in the molecular chain and the linkers and 19 valence electrons on each atom in the gold clusters. The remaining gold electrons are treated by an effective core potential (ECP).[44]

Transport Methods. Model geometries for the alkanes and silanes terminated with amine ($-NH_2-$) end groups are used in subsequent transport calculations where electronic currents are calculated using an NEGF/DFT formalism as implemented in *ATK2.0*.[45] In the NEGF/DFT calculations, the $Au_{20}-NH_2-(SiH_2)_n-NH_2-Au_{20}$ and $Au_{20}-NH_2-(CH_2)_n-NH_2-Au_{20}$ structures are each placed between single layers of 25 gold atoms on either side to allow for periodic DFT calculations. The DFT calculations are performed using the local density approximation (LDA) parametrized by Perdew and Zunger[46] with a single-ζ plus polarization basis set used for gold atoms and a double-ζ plus polarization basis set used for all other atoms.

Using the same atomic coordinates and reduced CRENBS ECP basis set with one active electron per gold atom, aug-cc-pVDZ basis for all carbon atoms, and relativistic Si-ECP (SEFIT,DF) basis set[47] with four active electrons per silicon atom, electron transport calculations are repeated using methods[31,32] in which the electronic structure of the tunnel junction is represented by a many-electron or configuration interaction (CI) expansion.[33,34] We compare the NEGF/DFT transport results with these many-electron correlated scattering (MECS) calculations for the alkanes with amine end groups performed in ref 39 and with MECS calculations performed within this work for the $Au_{20}-NH_2-(SiH_2)_n-NH_2-Au_{20}$ junctions.

For the MECS studies, structures optimized at the DFT level are used to generate a set of Hartree−Fock orbitals in *TURBOMOLE*.[42] These orbitals are used as the single-particle basis to generate the many-body bases for the CI calculations. To reduce the size of the configuration space in our many-body approach, ECPs leaving only the gold 6s electron[48] and the silicon $3s^23p^2$ valence electrons[47] explicitly treated are used in generating the Hartree−Fock orbitals. The Hartree−Fock orbital set is truncated by excluding all virtual orbitals with eigenvalues greater than 9.0 eV. The truncated molecular orbital set is used with the Monte Carlo configuration interaction (MCCI) selection procedure[33,34] to generate a many-electron basis set for the explicitly correlated transport calculations. A coefficient selection threshold of $c_{min} = 10^{-3}$ is used to generate CI vectors in the A_g singlet ground-state and the first excited singlet state in B_u symmetry. As voltage is applied, these two many-body states couple and allow the junction to polarize. The CI expansion vectors for the tunnel junctions with varying silane lengths contain from 5000 to 10 000 configuration state functions (CSFs). This level of correlation has been shown to be accurate for reproducing intermediate range electron correlations[49] that dominate correlation energies and seems adequate for molecular transport calculations.[31,32,37,39] These short CI expansions capture a large percentage of the correlation energy (resulting in accurate descriptions of electronic spectra[50,51]) as required to determine relative energy levels accurately in molecular junctions.

Tunnel Barrier Model. To gain a better understanding of end-group effects on the decay value β in alkane and silane systems, a simple tunnel barrier model is considered and complex band structures are calculated. In the tunnel barrier model, the tunnel current through a rectangular barrier can be written as:

$$I \propto \exp\left[-2l\sqrt{2\frac{m^*}{\hbar^2}\Phi_b}\right] \quad (2)$$

where l is the molecular length, m^* represents the effective mass of the charge carriers, and Φ_b is the barrier height. The barrier heights are estimated using the B3-LYP hybrid exchange correlation functional. Optimized structures from the earlier DFT/B3-LYP calculations are used. The highest occupied molecular orbital (HOMO) and lowest unoccupied molecular orbital (LUMO) energy levels for the alkane and silane diamines and dithiols bonded to the gold contacts are approximated by Kohn−Sham eigenvalues. Their energies are measured relative to the Fermi energy, which is taken to be the experimental work function for gold surfaces of $\epsilon_F = -5.1$ eV.[52] The potential energy barrier for electrons is approximated by the offset between the Fermi level and the LUMO state, whereas for hole transport the HOMO/Fermi-level offset is used to approximate the tunnel barrier height.

Bandstructures of 1D alkane and polysilane chains are computed to extract electron and hole effective masses from conduction and valence bands, respectively, via $m^* = (\hbar)^2(d^2E/dk^2)^{-1}$ evaluated at the band edge. The bandstructures are calculated by generating hydrogen-terminated molecules composed of either 20 $-CH_2-$ or $-SiH_2-$ units. DFT/B3-LYP calculations using the SV(P) basis set[43] are performed. From this calculation, a Kohn-Sham Hamiltonian matrix is extracted from the chain center to reduce finite length effects using four alkane or silane units. An infinite molecular wire is then generated by periodically repeating the extracted Hamiltonian

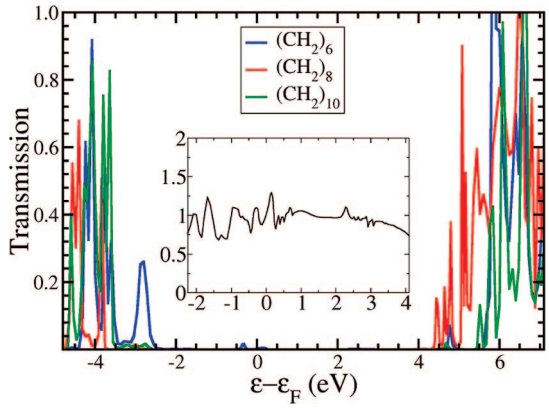

Figure 2. Transmission vs energy shifted from the Fermi energy for alkane diamines obtained from NEGF/DFT calculations. The inset shows a plot of the β decay values (per $-CH_2-$) vs a shift in the computational choice of the Fermi energy.

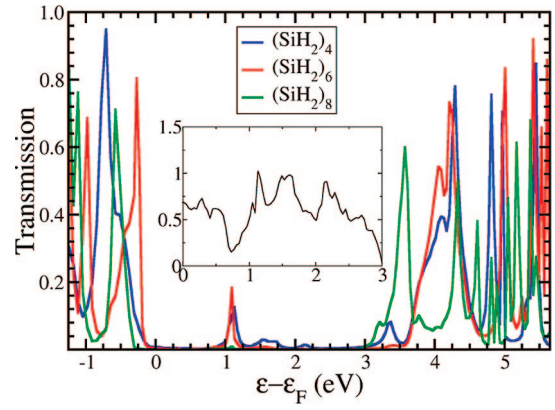

Figure 3. Transmission vs energy shifted by the Fermi energy for silane diamines obtained from NEGF/DFT calculations. The peaks in transmission near 1 eV are attributed to metal induced gap states (MIGS). The inset shows a plot of the β decay values vs a shift in the alignment of the Fermi energy. The β decay value varies greatly depending on the Fermi-level band alignment.

matrix, yielding infinite chains with a primitive cell that is double the normal size, yielding a lattice constant 2a.

Additionally, complex band structures are calculated to obtain more accurate values (as compared to the simple tunnel barrier model) for the exponential decay of the various chains.[53–55] Complex band-structure calculations yield the characteristic length of wave function decay for states in an energy gap along the molecular chains in a similar fashion to the decay exponent from the wave function inside the potential barrier. The nonresonant tunneling probability through a unit cell with lattice constant 2a is proportional to $e^{-2\beta a}$, or equivalently $e^{-4|Im(k)|a}$, where $k(E)$ is the momentum wavevector. The decay length β can be determined using $\beta(E) = 2\ Im\ k(E)$, and its value is dependent on the location of the Fermi level. The position of the Fermi level is determined using the same HOMO/Fermi-level offset discussed above for the simple tunnel barrier model.

III. Computational Results and Discussion

Fermi-Level Alignment. The alignment of the Fermi level relative to the bridging molecule's HOMO and LUMO in a metal−molecule−metal junction is extremely sensitive to charge transfer at the metal−molecule interface.[56–58] The use of DFT to describe the band alignment in metal−molecule−metal junctions has been studied widely,[24–30,54,56,59–63] and self-interaction errors as well as a lack of surface polarization response have been shown to yield incorrect transport properties, even in single-molecule junctions. In light of these issues, we have chosen to determine the alignment of the Fermi energy with the same procedure used for the Fermi-level alignment in the tunnel barrier model and the complex band-structure calculations described in Section II. Conductance values are determined using the equation for zero bias conductance:

$$G = g_0 T(E_F) \tag{3}$$

where g_0 is the fundamental unit of conductance, $2e^2/h = 77.5$ μS, and $T(E_F)$ is the transmission at the Fermi energy. Plots of the transmission for the alkane and silane diamines can be seen in Figures 2 and 3. In Figure 2, the alkane system shows a broad peak in the transmission plot in the HOMO−LUMO gap that can be attributed to metal-induced gap states (MIGS) from the Au_{20} clusters.[64] Because the Fermi level is sufficiently far from the bridging molecule's HOMO and LUMO, the decay constant β is relatively constant for a range of Fermi-energy shifts. In Figure 3, the silane system shows markedly different transmission properties. The HOMO−LUMO gap is much smaller than in the alkane case, and β and the conductance are much more dependent on the exact choice of Fermi level. The final Fermi energy for the alkane systems lies approximately 3−4 eV above the HOMOs for the three alkyl chains; this compares well with the 3 eV separation between the Fermi energy and alkyl chain valence band edge predicted by Prodan and Car.[54]

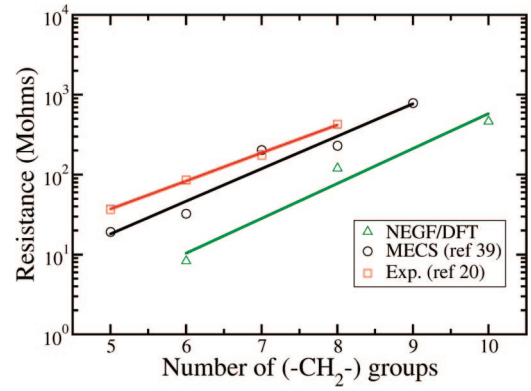

Figure 4. Resistance vs number of $-CH_2-$ groups in the alkane diamine systems. The theoretical results (NEGF/DFT and MECS) show good agreement with the experimental results[20] for this system with approximately equivalent β decay values (calculated from the slopes of the lines of least squares and given in Table 1).

Conductance Results. For alkane diamine tunnel junctions, the change in resistance as a function of the alkane length as predicted by different calculations is shown in Figure 4. Previous data from ref 39 using the MECS method[31,32] and results from our NEGF/DFT calculations using the same geometry as in the MECS study are shown. For comparison, experimental results from Venkataraman et al.[20] are also shown. From Figure 4, it is readily seen that the calculations are in good agreement with the experimental results for the alkane diamine tunnel junctions.

Previous calculations using the MECS method for the alkane diamine[39] and alkane dithiol[37] junctions found $\beta_C = 0.98/CH_2$ ($\beta = 0.76$ Å^{-1}) and $\beta_C = 0.50/CH_2$ ($\beta = 0.39$ Å^{-1}), respectively. Our NEGF/DFT approach found $\beta_C = 1.01/CH_2$ ($\beta = 0.78$ Å^{-1}) for the alkane diamine junctions, compared to $\beta_C = 0.93/CH_2$ from Wohlthat et al.[65] using an NEGF/DFT approach and $\beta_C = 0.82/CH_2$ from a semianalytical estimation by Prodan et al.[54] Earlier works by Müller,[11] Kaun et al.,[66] and Basch et al.[4] report β_C values of $1.24/CH_2$, $0.95/CH_2$, and $1.0/CH_2$ respectively for the alkane dithiol systems studied using the NEGF/DFT

TABLE 1: Experimental and Theoretical Decay Values β_C for Both Alkane Dithiols and Alkane Diamines

Amine End Group			
reference	β_C (per $-CH_2-$)	reference	β_C (per $-CH_2-$)
5 (experiment, HC[a])	0.81 ± 0.01	65 (theory)	0.93
5 (experiment, LC)	0.88 ± 0.03	MECS (ref 39)	0.98
20 (experiment)	0.91 ± 0.03	NEGF/DFT (this work)	1.01
54 (theory)	0.82		
Thiol End Group			
reference	β_C (per $-CH_2-$)	reference	β_C (per $-CH_2-$)
4 (theory)	1.0	17 (experiment, LC)	0.45 ± 0.09
5 (experiment, HC)	1.02 ± 0.14	21 (experiment)	1.0 ± 0.05
5 (experiment, LC)	1.08 ± 0.12	66 (theory)	0.95
9 (experiment)	1.07 ± 0.05	67 (experiment)	0.57 ± 0.03
11 (theory)	1.24	68 (experiment)	$0.68 - 0.79$
16 (experiment)	1.0	69 (experiment)	0.52 ± 0.05
17 (experiment, HC)	0.96 ± 0.15	MECS (ref 37)	0.50
17 (experiment, MC)	0.94 ± 0.05		

[a] For experimental data with multiple peaks in the conductance histogram, peaks are separated as HC for high conductance, MC for medium conductance, and LC for low conductance.

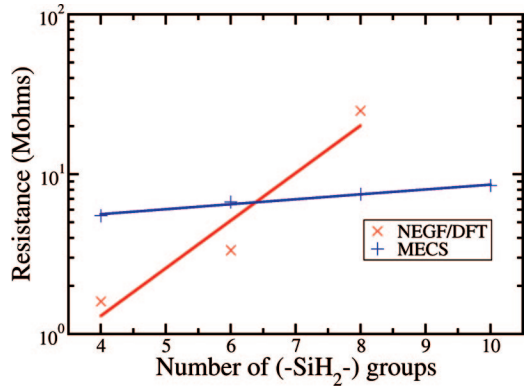

Figure 5. Resistance vs number of $-SiH_2-$ groups in the silane diamine systems. The NEGF/DFT results show a steeper slope and hence a larger β value than the MECS results ($\beta_{Si} = 0.69/SiH_2$ for the NEGF/DFT calculations compared with $\beta_{Si} = 0.14/SiH_2$ for the MECS method).

formalism. These are in good agreement with the measurements made for these tunnel junctions[5,16,17,20,21,67–69] as seen in Table 1. The contact geometry used in ref 11 for the alkane dithiol system differs from those used in ref 4 and ref 66; in ref 11, the dithiol linkers are bound to coordinatively unsaturated gold atoms above Au(111) surfaces (similar to the contact geometry for the amine-linked systems in this study), as opposed to the contact geometries in ref 4 and ref 66 in which the sulfur atoms lie above hollow sites on the gold surface. The above-atom geometry in ref 11 yields a 25% larger β_C value as compared with the above hollow-site binding geometries, thus illustrating the sensitivity of the transport properties to the exact junction geometry. Changing the S−Au binding geometry from above hollow site to above-atom has a comparable effect to changing the linking atom.

MECS calculations for the silane diamine junction yield a decay length $\beta_{Si} = 0.14/SiH_2$ ($\beta = 0.07$ Å^{-1}), whereas our NEGF/DFT calculations for the same junction yield $\beta_{Si} = 0.69/SiH_2$ ($\beta = 0.35$ Å^{-1}); the calculated resistances are plotted in Figure 5. Previously reported calculations for silane dithiol tunnel junctions with the CI transport approach yield β_{Si}=0.18/SiH_2 ($\beta = 0.09$ Å^{-1}).[37]

While to the best of our knowledge silane tunnel junctions have not been studied experimentally, methylated oligosilane chains in donor−bridge−acceptor (D−B−A) systems have been shown to exhibit a bridge attenuation factor of $\beta_{Si} = 0.37/Si$ ($\beta = 0.16$ Å^{-1}),[70] which falls in between our calculated values. The decay factor from electron-transfer data is obtained via a formula similar to eq 1:[71]

$$k = k_0 \exp(-\beta R_{DA}) \quad (4)$$

where k_0 is the rate constant at the reference distance, β is the length decay factor, and R_{DA} is the distance between the donor and acceptor minus the reference distance. In general, β values calculated from eq 4 will be dependent on the inter-site coupling strengths along the bridging molecule as well as the LUMO and energy differences between the bridge and the donor.[72,73] Interestingly, the β decay factor reported for the oligosilanes is closer to those reported for polyyne ($\beta = 0.10$ Å^{-1}) and polyene ($\beta = 0.08$ Å^{-1}) bridges[74] than those for alkanes. It should be noted, however, that β values below ~0.2 Å^{-1} in D−B−A systems may indicate a multistep hopping mechanism as opposed to a single-step tunneling mechanism;[75] the mechanism of charge transfer in silane chains would thus be somewhat ambiguous, whereas the mechanism in polyyne and polyene would likely be best described by hopping. Regardless of the mechanism, combined with the observed reduction in β relative to alkane chains seen in our calculations, these comparisons from electron-transfer data highlight the importance of σ-conjugation for transport in silanes. The reduced HOMO−LUMO gap in the silane chains due to the effects of σ-conjugation causes the decrease in β relative to the alkane chains, and it also could lead to the differences in the MECS and NEGF/DFT results. Correlation in silane chains has been shown to be greater than in alkane chains,[37] and the different treatments of correlation in the MECS and NEGF/DFT methods should therefore be more visible in the silane results.

Tunnel Barrier Model and Complex Band-Structure Results. Using the MECS approach, the inverse decay lengths for alkanes with different end groups differ by approximately a factor of 2, with $\beta_C = 0.98/CH_2$ for the alkane diamines and $\beta_C = 0.50/CH_2$ for the alkane dithiols. This is in contrast with experimental results, which indicate a steeper decay for the thiol end group.[5] This difference can be understood by considering the simple model of tunnel currents through a rectangular potential barrier described in eq 2. The HOMO and LUMO energies for the molecules between metal clusters are approximated as Kohn−Sham frontier orbital energies for alkane

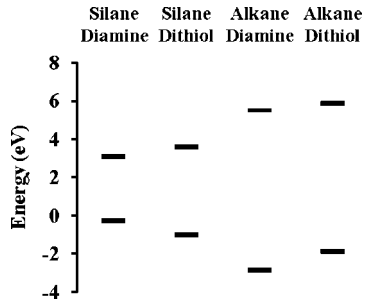

Figure 6. Molecular frontier energy levels for the hexane and hexasilane bonded to gold clusters via amine and thiol end groups. Energies levels are approximated by the Kohn−Sham eigenvalues from the DFT/B3LYP calculations described in the text. The zero of energy is taken to be the Fermi level approximated as the work function of gold (−5.1 eV).[52] The band gaps of the silane chains are much smaller than the band gaps of the alkane chains, leading to lower β decay values for the silanes.

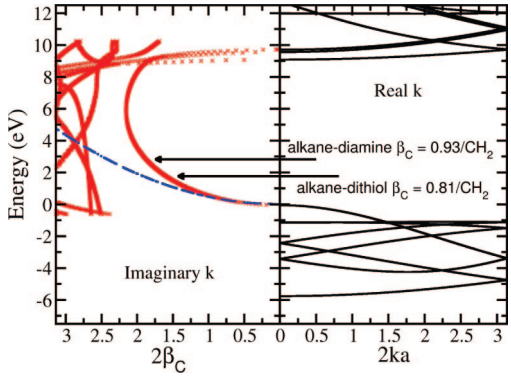

Figure 7. Band structure of the alkane chain for propagating states (solid lines) in the right panel and complex wavevectors of decaying wave functions (red crosses) in the left panel. The zero of the energy is taken at the top of the valence band with arrows indicating where the position of the Fermi energy should be located in alkane-based tunnel junctions with amine or thiol linkers. Only the complex wave vectors that lie within the HOMO−LUMO gap are shown. These correspond to two times the inverse decay length β_C of the probability density per $-CH_2-$ unit. The prediction of the rectangular potential barrier for alkanes is plotted with a blue dashed line for comparison.

diamine and dithiol, and for silane diamine and dithiol, and are plotted relative to the Fermi energy in Figure 6. Bandstructures of extended 1D alkane (compare to refs 54 and 55) and silane chains were also calculated and are plotted in Figures 7 and 8, respectively. The electron and hole effective masses are extracted from the bandstructures as described earlier and shown in Table 2.

The calculated effective mass for electrons in the alkanes is roughly three times the free-electron mass m_e and approximately an order of magnitude larger than the calculated effective mass for holes in alkanes of $0.3m_e$. The energy-level offsets for the hexanes (and hexasilanes) with the two different end groups considered in this work are displayed in Figure 6. The LUMO offsets relative to the Fermi level for these systems present a barrier of over 5 eV for tunneling electrons, whereas holes see a barrier of less than 3 eV. This is in agreement with the effective mass data in Table 2 for the alkane system, and we conclude that the electronic current across the alkanes is dominated by hole transport, as in other tunnel junctions.[58,66] Ignoring electrons as charge carriers, the hexane HOMO level offset relative to the Fermi level is used to approximate the tunnel barrier height, and for the purposes of our simple model analysis we assume that this is a representative barrier height

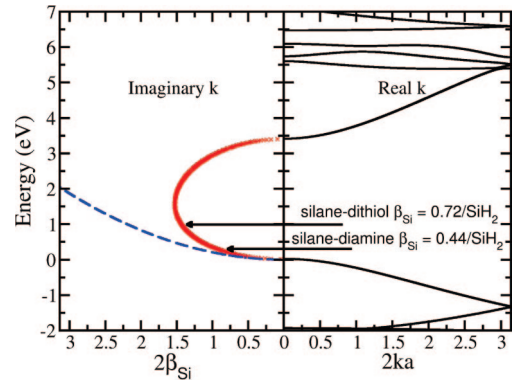

Figure 8. Similar to Figure 7, but for silicon hydride chains and silane-based tunnel junctions with amine or thiol linkers. The substantially decreased HOMO−LUMO gap size in the silanes, compared to the alkanes (Figure 7), makes the values of β_{Si} more sensitive to small differences in the Fermi-level alignment.

TABLE 2: Electron and Hole Effective Masses for Infinite Length Alkane and Silane Chains as Extracted from Band-Structure Calculations

	alkane	silane
m_e*	$3.03m_e$[a]	$0.22m_e$
m_h*	$0.30m_e$	$0.31m_e$

[a] m_e denotes the free-electron mass.

for all of the alkane lengths considered. For the alkane diamines, the HOMO-Fermi-level offset is 2.83 eV, close to the previously reported value of 3 eV,[54] and larger than the estimated HOMO-Fermi offset for alkane dithiols of 1.84 eV computed in an earlier work.[37] These energy offsets are marked by the arrows in Figure 7. By the position of the arrows in Figure 7, we see that this simple potential barrier model qualitatively agrees with the MECS results, which predict a larger β value for the amine-linked alkanes compared to the thiol-linked ones (in contrast to the experimental results). Using the tunnel barrier model and the previous discussion of Fermi-level alignment, one can understand why the disagreement with experiment occurs. A moderate shift of the Fermi level away from the HOMO of the alkane dithiol could potentially change the predicted trend of the β decay values. This shift could occur with a more exact treatment of the electronic charge transfer between the molecule and the metal surface[56] or by treating systems with slightly different contact geometries at the metal−molecule interface.[11]

Complex band-structure calculations for alkane diamines (Figure 7) yielded an inverse decay length of $\beta_C = 0.93/CH_2$, which is in surprisingly good agreement with the direct calculations of the tunnel current. The inverse decay length for alkane dithiols of $\beta_C = 0.81/CH_2$ is lower than the decay value $\beta_C = 1.0/CH_2$ obtained by Tomfohr et al.[55] As with the simple potential barrier model, this is likely due to the different techniques used in determining the position of the Fermi level relative to the HOMO and LUMO of the alkane chain. The size of the difference between the decay values highlights the sensitivity of the method to Fermi-level alignment. An additional source of disagreement between experimental results and the complex band-structure results could arise from the neglect of the sulfur contribution to the molecular HOMO in the band-structure model (cf. Supporting Information).[53,76]

The simple model of electron tunneling through a potential barrier can also be applied to provide a better understanding of the silane systems. The inverse decay lengths β obtained for silanes from the MECS transport calculations are similar in

magnitude with $\beta_{Si} = 0.14/SiH_2$ ($\beta = 0.07$ Å^{-1}) for silane diamines and $\beta_{Si} = 0.18/SiH_2$ ($\beta = 0.09$Å^{-1}) for silane dithiols. Because of the reduction of the silane band gap relative to the alkane band gap, we are limited to a qualitative discussion of the observed values of β; the smaller band gap makes the tunnel currents much more sensitive to the approximations made to estimate the tunnel barriers. For the silanes, electron and hole effective masses are of the same order of magnitude with an electron effective mass equal to $0.22m_e$, compared to the hole effective mass of $0.31m_e$. It is found that there is some molecular contribution to the HOMOs of the gold cluster-derived states, which lie around 1.01 and 0.27 eV below the Fermi energy for hexasilane with thiol and amine linkers, respectively. In this case, the Fermi level is not in a midgap position, but the molecular HOMO states are aligned close to the Fermi level (as seen from Figure 6). This suggests that the transport is predominately through the HOMO state of the molecule with hole transport dominating the current. The larger potential barrier for hole transport in the silane dithiol systems is consistent with a slightly higher value of β for the thiol-bridged silanes relative to the amine terminated silanes.

Complex band-structure calculations for silanes confirm the predictions of the simple square barrier analysis, as shown in Figure 8. The silane complex band structures yield $\beta_{Si} = 0.44/SiH_2$ for the diamine linked and $\beta_{Si} = 0.72/SiH_2$ for the dithiol linked. The discrepancies between the NEGF/DFT, complex band structure, and MECS results are likely related to the increased importance of correlation in the silane systems and the differences in how the transport methods compute the electronic structure of the systems (DFT with the LDA/PZ exchange correlation functional for NEGF, DFT with the B3-LYP hybrid exchange correlation functional for band structure, and CI for MECS). The trend observed for the reduction in the β values for the silanes relative to the alkanes is consistent with the simple tunnel barrier model and the complex band-structure analysis. However, the analysis also points out that the exact β values for the silanes are sensitive to small errors in the energy-level alignments. This can be seen in Figure 8 where the complex band connecting the valence and conduction bands of the silane systems falls away more steeply from the band edges than the analogous complex band for the alkanes in Figure 7.

IV. Conclusions

A comparative study between an NEGF/DFT method and an MECS formalism for transport in oligoalkane and oligosilane single-molecule transport junctions has been conducted. Conductance values of metal−molecule−metal junctions in which gold electrodes are bridged by alkane and silane diamines and dithiols have been computed using both methods, and the results were interpreted using both a simple potential barrier model and complex band-structure calculations. Conductance results from both the NEGF/DFT and MECS methods and from experiment agree well for the alkane diamine system. For the alkane dithiol system, inverse decay lengths calculated from MECS and NEGF/DFT methods disagree. The source of the disagreement is likely from the different methods used for handling charge transfer at the metal−molecule interface, which has a strong effect on the band alignment. In the case of silane diamine, the NEGF/DFT method yields a higher value for the inverse decay length β compared to the MECS results. The values fall on either side of the experimental result estimated from electron-transfer reactions.[70] The discrepancy in β values between the two methods could be due in part to the different techniques used to treat correlation between the two formalisms.

The energy-level alignment is found to be critical in all systems for accurately determining end-group effects and inverse decay lengths. Of the four systems studied, the alkane diamine junctions seem to have the most tolerance for error in band alignment, partly due to the large HOMO−LUMO gap and partly due to the nature of the charge transfer between the gold electrode and amine linker. Because the silanes have smaller HOMO−LUMO gaps, errors in the band alignment for these systems are magnified and the inverse decay length is found to be extremely dependent on the exact Fermi-energy position.

In both methods, the silane inverse decay length is found to be lower than that of the alkane decay value, indicating that σ-bond delocalization may be another means by which to tailor molecular electronic properties, serving as an intermediate between π-conjugated and nonconjugated systems. This could serve as another potential tool in the tool kit of molecular transport engineering.

Acknowledgment. This work has been partially supported by Science Foundation Ireland and U.S. International NSF Grant No. DMR-0353831/003. C.G. is supported by a Graduate Research Fellowship from the NSF. The authors thank S. Yeganeh for useful discussions, and ATK for the use of *ATK 2.0*.

Supporting Information Available: A table of contact resistances extrapolated from experimental results compared with contact resistances calculated by the NEGF/DFT and MECS methods is available, and a plot of the partial density of states (PDOS) projected on one of the linking sulfur atoms in a hexanedithiol bridging molecule is provided to demonstrate the contribution of the sulfur atoms to the molecular HOMO in a tunnel junction. This material is available free of charge via the Internet at http://pubs.acs.org.

References and Notes

(1) Cuniberti, G.; Fagas, G.; Richter, K. Introducing Molecular Electronics: A Brief Overview. In Introducing Molecular Electronics; 2005; p 1.
(2) Nitzan, A.; Ratner, M. A. *Science* **2003**, *300*, 1384.
(3) Tao, N. J. *Nature Nanotechnol.* **2006**, *1*, 173.
(4) Basch, H.; Cohen, R.; Ratner, M. A. *Nano Lett.* **2005**, *5*, 1668.
(5) Chen, F.; Li, X. L.; Hihath, J.; Huang, Z. F.; Tao, N. J. *J. Am. Chem. Soc.* **2006**, *128*, 15874.
(6) Grigoriev, A.; Skoldberg, J.; Wendin, G.; Crljen, Z. *Phys. Rev. B* **2006**, *74*, 045401.
(7) Kim, G.; Wang, S. C.; Lu, W. C.; Nardelli, M. B.; Bernholc, J. *J. Chem. Phys.* **2008**, *128*, 024708.
(8) Lee, M. H.; Speyer, G.; Sankey, O. F. *Phys. Status Solidi B* **2006**, *243*, 2021.
(9) Li, X. L.; He, J.; Hihath, J.; Xu, B. Q.; Lindsay, S. M.; Tao, N. J. *J. Am. Chem. Soc.* **2006**, *128*, 2135.
(10) Martin, C. A.; Ding, D.; van der Zant, H. S. J.; van Ruitenbeek, J. M. *New J. Phys.* **2008**, *10*, 065008.
(11) Muller, K. H. *Phys. Rev. B* **2006**, *73*, 045403.
(12) Xue, Y. Q.; Ratner, M. A. *Phys. Rev. B* **2003**, *68*, 115407.
(13) Xue, Y. Q.; Ratner, M. A. *Phys. Rev. B* **2004**, *69*, 085403.
(14) Zhu, X. Y. *J. Phys. Chem. B* **2004**, *108*, 8778.
(15) Bumm, L. A.; Arnold, J. J.; Dunbar, T. D.; Allara, D. L.; Weiss, P. S. *J. Phys. Chem. B* **1999**, *103*, 8122.
(16) Jang, S. Y.; Reddy, P.; Majumdar, A.; Segalman, R. A. *Nano Lett.* **2006**, *6*, 2362.
(17) Li, C.; Pobelov, I.; Wandlowski, T.; Bagrets, A.; Arnold, A.; Evers, F. *J. Am. Chem. Soc.* **2008**, *130*, 318.
(18) Petta, J. R.; Salinas, D. G.; Ralph, D. C. *Appl. Phys. Lett.* **2000**, *77*, 4419.
(19) Suzuki, M.; Fujii, S.; Wakamatsu, S.; Akiba, U.; Fujihira, M. *Nanotechnology* **2004**, *15*, S150.
(20) Venkataraman, L.; Klare, J. E.; Tam, I. W.; Nuckolls, C.; Hybertsen, M. S.; Steigerwald, M. L. *Nano Lett.* **2006**, *6*, 458.
(21) Xu, B. Q.; Tao, N. J. J. *Science* **2003**, *301*, 1221.
(22) Choi, S. H.; Kim, B.; Frisbie, C. D. *Science* **2008**, *320*, 1482.

(23) Datta, S. Quantum Transport: Atom to Transistor; Cambridge University Press: New York, 2005.
(24) Evers, F.; Weigend, F.; Koentopp, M. *Phys. Rev. B* **2004**, *69*, 235411.
(25) Ke, S. H.; Baranger, H. U.; Yang, W. T. *J. Chem. Phys.* **2007**, *126*, 201102.
(26) Koentopp, M.; Burke, K.; Evers, F. *Phys. Rev. B* **2006**, *73*, 121403.
(27) Neaton, J. B.; Hybertsen, M. S.; Louie, S. G. *Phys. Rev. Lett.* **2006**, *97*, 216405.
(28) Thygesen, K. S. *Phys. Rev. Lett.* **2008**, *100*, 166804.
(29) Toher, C.; Filippetti, A.; Sanvito, S.; Burke, K. *Phys. Rev. Lett.* **2005**, *95*, 146402.
(30) Toher, C.; Sanvito, S. *Phys. Rev. B* **2008**, *77*, 155402.
(31) Delaney, P.; Greer, J. C. *Int. J. Quantum Chem.* **2004**, *100*, 1163.
(32) Delaney, P.; Greer, J. C. *Phys. Rev. Lett.* **2004**, *93*, 036805.
(33) Greer, J. C. *J. Chem. Phys.* **1995**, *103*, 1821.
(34) Greer, J. C. *J. Comput. Phys.* **1998**, *146*, 181.
(35) Fogarty, H. A.; Casher, D. L.; Imhof, R.; Schepers, T.; Rooklin, D. W.; Michl, J. *Pure Appl. Chem.* **2003**, *75*, 999.
(36) Miller, R. D.; Michl, J. *Chem. Rev.* **1989**, *89*, 1359.
(37) Fagas, G.; Delaney, P.; Greer, J. C. *Phys. Rev. B* **2006**, *73*, 241314.
(38) Larsson, J. A.; Nolan, M.; Greer, J. C. *J. Phys. Chem. B* **2002**, *106*, 5931.
(39) Fagas, G.; Greer, J. C. *Nanotechnology* **2007**, *18*, 424010.
(40) Becke, A. D. *J. Chem. Phys.* **1993**, *98*, 5648.
(41) Stephens, P. J.; Devlin, F. J.; Chabalowski, C. F.; Frisch, M. J. *J. Phys. Chem.* **1994**, *98*, 11623.
(42) Ahlrichs, R.; Bar, M.; Haser, M.; Horn, H.; Kolmel, C. *Chem. Phys. Lett.* **1989**, *162*, 165.
(43) Weigend, F.; Haser, M.; Patzelt, H.; Ahlrichs, R. *Chem. Phys. Lett.* **1998**, *294*, 143.
(44) Ross, R. B.; Powers, J. M.; Atashroo, T.; Ermler, W. C.; Lajohn, L. A.; Christiansen, P. A. *J. Chem. Phys.* **1990**, *93*, 6654.
(45) Brandbyge, M.; Mozos, J. L.; Ordejon, P.; Taylor, J.; Stokbro, K. *Phys. Rev. B* **2002**, *65*, 165401.
(46) Perdew, J. P.; Zunger, A. *Phys. Rev. B* **1981**, *23*, 5048.
(47) Igelmann, G.; Stoll, H.; Preuss, H. *Mol. Phys.* **1988**, *65*, 1321.
(48) Fuentealba, P.; Stoll, H.; Vonszentpaly, L.; Schwerdtfeger, P.; Preuss, H. *J. Phys. B: At., Mol. Opt. Phys.* **1983**, *16*, L323.
(49) Prendergast, D.; Nolan, M.; Filippi, C.; Fahy, S.; Greer, J. C. *J. Chem. Phys.* **2001**, *115*, 1626.
(50) Gyoffry, W.; Bartlett, R. J.; Greer, J. C. *J. Chem. Phys.* **2008**, *129*, 064103.
(51) Larsson, J. A.; Tong, L.; Cheng, T.; Nolan, M.; Greer, J. C. *J. Chem. Phys.* **2001**, *114*, 15.
(52) Hansen, W. N.; Johnson, K. B. *Surf. Sci.* **1994**, *316*, 373.
(53) Fagas, G.; Kambili, A.; Elstner, M. *Chem. Phys. Lett.* **2004**, *389*, 268.
(54) Prodan, E.; Car, R. *Nano Lett.* **2008**, *8*, 1771.
(55) Tomfohr, J. K.; Sankey, O. F. *Phys. Rev. B* **2002**, *65*, 245105.
(56) Stadler, R.; Jacobsen, K. W. *Phys. Rev. B* **2006**, *74*, 161405.
(57) Tian, W. D.; Datta, S.; Hong, S. H.; Reifenberger, R.; Henderson, J. I.; Kubiak, C. P. *J. Chem. Phys.* **1998**, *109*, 2874.
(58) Xue, Y. Q.; Datta, S.; Ratner, M. A. *J. Chem. Phys.* **2001**, *115*, 4292.
(59) Koentopp, M.; Chang, C.; Burke, K.; Car, R. *J. Phys.: Condens. Matter* **2008**, *20*, 083203.
(60) Quek, S. Y.; Venkataraman, L.; Choi, H. J.; Louie, S. G.; Hybertsen, M. S.; Neaton, J. B. *Nano Lett.* **2007**, *7*, 3477.
(61) Reimers, J. R.; Cai, Z. L.; Bilic, A.; Hush, N. S. The Appropriateness of Density-Functional Theory for the Calculation of Molecular Electronics Properties. In Molecular Electronics III; 2003, Vol. 1006, 235.
(62) Toher, C.; Sanvito, S. *Phys. Rev. Lett.* **2007**, *99*, 056801.
(63) Wang, J. G.; Prodan, E.; Car, R.; Selloni, A. *Phys. Rev. B* **2008**, *77*, 245443.
(64) Crljen, Z.; Grigoriev, A.; Wendin, G.; Stokbro, K. *Phys. Rev. B* **2005**, *71*, 165316.
(65) Wohlthat, S.; Pauly, F.; Reimers, J. R. *Chem. Phys. Lett.* **2008**, *454*, 284.
(66) Kaun, C. C.; Guo, H. *Nano Lett.* **2003**, *3*, 1521.
(67) Cui, X. D.; Primak, A.; Zarate, X.; Tomfohr, J.; Sankey, O. F.; Moore, A. L.; Moore, T. A.; Gust, D.; Nagahara, L. A.; Lindsay, S. M. *J. Phys. Chem. B* **2002**, *106*, 8609.
(68) Akkerman, H. B.; Blom, P. W. M.; de Leeuw, D. M.; de Boer, B. *Nature* **2006**, *441*, 69.
(69) Haiss, W.; Nichols, R. J.; van Zalinge, H.; Higgins, S. J.; Bethell, D.; Schiffrin, D. J. *PCCP* **2004**, *6*, 4330.
(70) Sasaki, M.; Shibano, Y.; Tsuji, H.; Araki, Y.; Tamao, K.; Ito, O. *J. Phys. Chem. A* **2007**, *111*, 2973.
(71) Closs, G. L.; Miller, J. R. *Science* **1988**, *240*, 440.
(72) Eng, M. P.; Albinsson, B. *Angew. Chem., Int. Ed.* **2006**, *45*, 5626.
(73) Ratner, M. A. *J. Phys. Chem.* **1990**, *94*, 4877.
(74) Osuka, A.; Tanabe, N.; Kawabata, S.; Yamazaki, I.; Nishimura, Y. *J. Org. Chem.* **1995**, *60*, 7177.
(75) Berlin, Y. A.; Grozema, F. C.; Siebbeles, L. D. A.; Ratner, M. A. *J. Phys. Chem. C* **2008**, *112*, 10988.
(76) Tomfohr, J. K.; Sankey, O. F. *Phys. Status Solidi B* **2002**, *233*, 59.

JP8078698